The Astrophysical Journal, 833:33 (16pp), 2016 December 10 doi:10.3847/1538-4357/833/1/33
© 2016. The American Astronomical Society. All rights reserved.

THE SLOAN DIGITAL SKY SURVEY REVERBERATION MAPPING PROJECT: BIASES IN $z > 1.46$ REDSHIFTS DUE TO QUASAR DIVERSITY

K. D. Denney[1,2,11], Keith Horne[3], W. N. Brandt[4,5,6], C. J. Grier[4,5], Luis C. Ho[7,8], B. M. Peterson[1,2,9], J. R. Trump[4,12], and J. Ge[10]

[1] Department of Astronomy, The Ohio State University, 140 West 18th Avenue, Columbus, OH 43210, USA; denney@astronomy.ohio-state.edu
[2] Center for Cosmology and AstroParticle Physics, The Ohio State University, 191 West Woodruff Avenue, Columbus, OH 43210, USA
[3] SUPA Physics & Astronomy, University of St. Andrews, St. Andrews KY16 9SS, UK
[4] Department of Astronomy & Astrophysics, 525 Davey Lab, The Pennsylvania State University, University Park, PA 16802, USA
[5] Institute for Gravitation and the Cosmos, The Pennsylvania State University, University Park, PA 16802, USA
[6] Department of Physics, 104 Davey Lab, The Pennsylvania State University, University Park, PA 16802, USA
[7] Kavli Institute for Astronomy and Astrophysics, Peking University, Beijing 100871, China
[8] Department of Astronomy, School of Physics, Peking University, Beijing 100871, China
[9] Space Telescope Science Institute, 3700 San Martin Drive, Baltimore, MD 21218, USA
[10] Astronomy Department University of Florida 211 Bryant Space Science Center P.O. Box 112055 Gainesville, FL 32611-2055, USA
Received 2016 May 25; revised 2016 September 23; accepted 2016 October 9; published 2016 December 6

ABSTRACT

We use the coadded spectra of 32 epochs of Sloan Digital Sky Survey (SDSS) Reverberation Mapping Project observations of 482 quasars with $z > 1.46$ to highlight systematic biases in the SDSS- and Baryon Oscillation Spectroscopic Survey (BOSS)-pipeline redshifts due to the natural diversity of quasar properties. We investigate the characteristics of this bias by comparing the BOSS-pipeline redshifts to an estimate from the centroid of He II λ1640. He II has a low equivalent width but is often well-defined in high-S/N spectra, does not suffer from self-absorption, and has a narrow component which, when present (the case for about half of our sources), produces a redshift estimate that, on average, is consistent with that determined from [O II] to within the He II and [O II] centroid measurement uncertainties. The large redshift differences of $\sim$1000 km s^{-1}, on average, between the BOSS-pipeline and He II-centroid redshifts, suggest there are significant biases in a portion of BOSS quasar redshift measurements. Adopting the He II-based redshifts shows that C IV does not exhibit a ubiquitous blueshift for all quasars, given the precision probed by our measurements. Instead, we find a distribution of C IV-centroid blueshifts across our sample, with a dynamic range that (i) is wider than that previously reported for this line, and (ii) spans C IV centroids from those consistent with the systemic redshift to those with significant blueshifts of thousands of kilometers per second. These results have significant implications for measurement and use of high-redshift quasar properties and redshifts, and studies based thereon.

Key words: galaxies: active – galaxies: distances and redshifts – galaxies: nuclei – quasars: emission lines – quasars: general – quasars: supermassive black holes

1. INTRODUCTION

Mapping the location of stars and galaxies as a function of distance—or redshift—helps us understand not only the content of the universe but also its structure and evolution and the physical principles shaping what we observe. Quasars, or active galactic nuclei (AGNs; used synonymously in this work), are arguably the most useful extragalactic sources for mapping the universe at high redshift. These accreting supermassive black holes (BHs) can outshine their host galaxies by several orders of magnitude and are thus observable at much greater distances than their quiescent counterparts. Moreover, quasar spectra are characterized by the presence of high equivalent width (EW) emission lines distributed across UV to NIR wavelengths. These emission lines can be identified and redshifts determined even with relatively low-S/N, resource-economic, "survey-quality" spectra. Several large surveys have been obtaining large numbers of quasar spectra for cosmological studies, such as measurements of baryon acoustic oscillations (e.g., Busca et al. 2013; Delubac et al. 2015). The Sloan Digital Sky Survey (SDSS) alone, with programs such as the Baryon Oscillation Spectroscopic Survey (BOSS), has spectroscopically confirmed $\sim$370,000 quasars (York et al. 2000; Schneider et al. 2010; Dawson et al. 2013; Pâris et al. 2014).

These quasar redshifts are invaluable for studies on both large and small scales, both for studies directly related to the quasars and for those reliant upon the intervening absorption. However, making accurate redshift measurements of quasars, particularly at high redshifts, is surprisingly difficult—an issue that is, perhaps, not broadly known or appreciated outside the direct quasar physics community. Quasar spectra are a blended superposition of many emission and absorption components that arise from physically distinct sources at different distances from the BH. Components include the thermal continuum from the accretion disk, narrow and broad emission lines from the narrow-line region (NLR) and broad-line region (BLR), respectively, intrinsic and intervening absorption lines, and host-galaxy starlight. Of these emission- and absorption-line components, some are better suited for redshift determinations than others.

Associated quasar absorption lines are usually attributed to outflows from the nucleus and are not expected to lie at the systemic redshift. Host-galaxy stellar absorption features, on the other hand, are the most robust measure of the galaxy's redshift. Unfortunately, these absorption lines are generally

[11] NSF Astronomy & Astrophysics Postdoctoral Fellow.
[12] Hubble Fellow.

masked by the luminous quasar contributions. Even if observable, rest-frame optical lines, such as Ca II H & K lines at $\lambda\lambda$ 3969, 3934, are inaccessible in optical spectra of high-redshift quasars.

In the absence of reliable absorption lines, quasar redshifts are best determined from narrow emission lines that arise from the NLR or the host galaxy. Of particular interest are lines due to forbidden transitions that cannot arise in the high-density and high-velocity BLR environment, and so are not blended with a broad-line component or severely susceptible to dynamics dominated by the nuclear activity. The narrow lines are still sometimes observed to have small blueshifts ($\sim$10–100 km s^{-1}) compared to host-galaxy absorption lines, and this effect may have a luminosity dependence (see, e.g., Shen et al. 2016; Woo et al. 2016). Unfortunately, using high-EW, isolated, narrow forbidden lines also becomes difficult using optical spectra of high-redshift quasars because rest-frame UV forbidden emission lines have much smaller EWs, and, at the highest redshifts ($z \gtrsim 3$), the only NLR emission lines visible in optical spectra are due to permitted transitions that are blended with BLR emission, have relatively low EW, and are often resonance transitions susceptible to self-absorption, e.g., Lyα, C IV λ1549, or He II λ1640.

If absorption and narrow emission lines cannot be used for redshifts, the broad emission lines are used. This is most often required at high redshifts, where the other methods are no longer suitable. Difficulties in measuring redshifts based on these lines arise first from fundamental difficulties with either the specific transition or data quality (or both). First, the strong UV lines (Lyα, C IV, C III], and Mg II) are all either resonance lines susceptible to self-absorption, and/or are heavily blended with other species or within a multiplet. The line ratios within these blends and multiplets depend on physical properties of the nuclear environment, such as optical depth, density, and incident ionizing radiation (e.g., Baldwin et al. 1995; Korista et al. 1997; Casebeer et al. 2006). There is also the possibility that the dynamics of the gas deep within the potential well of the BH systematically shifts the center or peak of the broad lines away from wavelength expected for the true, systemic redshift of the quasar. As we will see from investigations described in this work, broad-line-only-based redshifts are more complicated than other redshift determinators, and while they can be reliable in some objects, they have the capability of being systematically uncertain by very large amounts, even thousands of kilometers per second, with high-ionization broad lines less reliable, on average, than low-ionization broad lines.

Known velocity shifts between different quasar emission lines are another challenge that contributes to biases in redshifts (e.g., see Shen et al. 2016, and discussion and references therein). Several studies have already explored biases in the SDSS-pipeline redshifts (e.g., Hewett & Wild 2010, hereafter HW10). While they still utilize cross-correlation with a master template, HW10 improve the SDSS redshift estimates of quasars by building a redshift "ladder" as a function of increasing redshift, since the redshifts of more nearby quasars can be more accurately determined from host-galaxy stellar features and strong forbidden, narrow emission lines. HW10 and Shen et al. (2016) find trends in line-to-line velocity shifts with quasar luminosity. While luminosity is an easily measured observable, more in-depth analyses of the spectral diversity of quasars from eigenvector analysis (see Boroson & Green 1992) suggest that the largest source of emission-line diversity in quasars, dubbed "Eigenvector 1" (EV1), is more likely related to accretion rate and the quasar spectral energy distribution (SED). EV1 analysis—based on a principal component analysis (PCA) of measured properties of quasar emission lines and continuum emission—shows that the relative strengths of different emission lines and the velocity shifts between lines seem to be well-correlated (e.g., Baskin & Laor 2005). In flux-limited surveys, luminosity can be a reasonable proxy for accretion rate, potentially leading to the luminosity correlation found by HW10 and others. This connection is a concern for redshifts based on composite quasar spectra formed from flux-limited samples, as the composite will be weighted toward the spectral properties associated with the relatively higher luminosity quasars.

SDSS-I/II-pipeline redshifts[13] (hereafter SDSS-pipeline) are based on either emission-line matching or cross-correlation with the Vanden Berk et al. (2001) composite quasar spectrum. While using a composite spectrum formed from many thousands of survey-quality quasar spectra will provide a very high S/N template, it does not account for the intrinsic diversity in the physical structure, environment, and SED among quasars that we can infer from the range of observed spectroscopic differences. It will thus create biases in the redshifts of objects with properties different from the average properties of the quasars used in its creation. Of particular importance is understanding (i) the physical properties that modify the structure of the emission lines, and (ii) on what observable variables those physical properties depend. One challenge is that the SDSS pipeline assumes only a single wavelength for many multiplets and/or highly blended transitions in the UV for its emission-line matching and line identification. This assumption combined with diversity in the spectral structure of individual quasars (i.e., differences in multiplet ratios for those with relatively wide velocity separation) could easily contribute systematic uncertainties in the determined redshifts beyond those typically quoted based on [O III] or Mg II ($\sim$50–300 km s^{-1}; Shen et al. 2011).

Redshift estimates from the BOSS pipeline (Bolton et al. 2012), which we utilize in this work, also use an eigenvector PCA method that, unlike the Boroson & Green (1992) analysis of quasar properties, is based on a spectral, or pixel-based, analysis of the BOSS quasar sample, and is more sophisticated than the previous SDSS-pipeline cross-correlation redshifts. Cross-correlation and PCA analysis should both be more robust against biases due to small, intrinsic velocity shifts between lines (Shen et al. 2016) than using individual emission lines to determine the redshift because these methods average over all shifts. Additionally, the PCA-based redshifts should be even more robust than cross-correlation with a single composite spectrum because a template built for each quasar is not as susceptible to the "averaging" biases from using a single quasar template. However, the BOSS PCA templates are built using training-set spectra with redshifts determined from the original SDSS method. As such, while the BOSS PCA method is more sophisticated overall (see also Dawson et al. 2016 for continued improvements), redshift biases (see, e.g., Font-Ribera et al. 2013; Pâris et al. 2014) may have propagated into the templates due to redshift inaccuracies in the training set spectra.

[13] See http://classic.sdss.org/dr7/algorithms/redshift_type.html.

Here, we investigate the possibility of systematic errors in the redshifts of BOSS quasars due to quasar diversity effects, which we define primarily to be the observed spectroscopic differences between quasar emission line properties. Of particular interest here are the relative velocity shifts and line ratios between different emission lines. However, using the Boroson & Green (1992) EV1 parameter space and related investigations, the observed spectroscopic differences seem to be traceable to a physical parameter space. Although this connection is not yet well-established and an in-depth study of this is not the goal of this work, we may also use "quasar diversity" to indicate either the observed spectroscopic differences, the intrinsic physical origin that likely causes the observed difference, or the possible connection between the two. If an observed versus physical distinction is important and necessary when discussing quasar diversity, we will refer to the observed spectral differences as spectroscopic diversity and the implied physical differences as physical diversity and/or EV1 effects. For this analysis, we use BOSS spectra that were taken as part of the SDSS Reverberation Mapping (SDSS-RM) Project from which we analyze properties of two narrow emission lines observable in optical spectra of intermediate- and high-redshift quasars. Our investigation is laid out as follows. In Section 2 we present the SDSS-RM Project data that we use for this investigation. Section 3 describes our analysis of these data for measuring the redshifts from He II λ1640 and the [O II] λ3727 doublet, and in Section 4 we discuss our results. Final remarks on our results are made in Section 5.

2. DATA

The SDSS-RM Project is spectroscopically monitoring broad-line quasars in a single 7 deg^2 field (the CFHT-LS W3 field) with the SDSS telescope's (Gunn et al. 2006) BOSS spectrograph (Smee et al. 2013). Here, we utilize the data obtained from the SDSS-III (Eisenstein et al. 2011) ancillary program between 2014 January and July. Covering redshifts over the range $0.1 < z < 4.5$, the SDSS-RM sample consists of 849 quasars with a flux limit of $i_{\rm psf} = 21.7$ mag. Each of the 32 epochs of observations was a $\sim$2 hr exposure taken during dark/gray time, with an average cadence of $\sim$4 days over this $\sim$6 month period. The technical overview of this program is provided by Shen et al. (2015).

Here we use the subsample of Denney et al. (2016) to study the properties of the C IV λ1549 emission-line region. The sample consists only of quasars with $z > 1.46$, where objects were removed that obstructed the C IV analysis, such as a few with very low C IV EW and several additional objects with broad absorption lines (see Denney et al. 2016, for further sample selection details). The final sample consists of 482 sources. For this analysis, we use only the high-S/N, continuum-subtracted "coadded" spectrum of each source. This was made by combining all good epochs using the latest BOSS spectroscopic pipeline `idlspec2d` (see Shen et al. 2015, and D. Schlegel et al. 2016, in preparation) and then subtracting the AGN continuum, which was linearly fit using wavelength regions $\sim$1450 and $\sim$1700 Å. Most (405) quasars have all 32 epochs of spectra included in the coadd, and only 9 have more than 3 (10%) epochs discarded. Figure 1, reproduced from Denney et al. (2016), shows the redshift and $i_{\rm psf}$ magnitude distribution of our sample.

3. SPECTROSCOPIC ANALYSIS: MEASURING EMISSION-LINE-BASED REDSHIFTS

The redshifts for our sample, as determined from the BOSS pipeline (Bolton et al. 2012), are likely already a moderate improvement over typical BOSS-pipeline redshifts because we are able to use the coadded spectra (see Shen et al. 2015), as opposed to the individual, lower-S/N single-epoch spectra (although Denney et al. 2016 and Shen et al. 2016 find that line centroid measurements, and thus emission-line cross correlations, are relatively more robust in the presence of spectral noise than other measured emission-line properties). However, the real advantage afforded by this relatively higher-S/N sample is to enable the analysis of low-EW narrow emission lines, not otherwise reliably detected in low-S/N spectra, to study the effects of intrinsic quasar spectroscopic diversity on the redshift determinations. We compare redshifts determined using the He II λ1640 emission line, which *is* susceptible to shifts in its observed line properties due to spectroscopic diversity (likely related to EV1 effects; see, e.g., Richards et al. 2011, hereafter R11), and [O II] λ3727 which, presumably, is *not*.

He II is not a resonance line and therefore not susceptible to self-absorption, and intervening absorption affects only a small percentage of objects. It is also a more isolated transition than many UV lines, so that blending is less of a concern. This makes it a more favorable line for studying the effects of quasar diversity on redshift determinations. However, there are two potential problems. First, while we would ideally isolate and study the NLR component of He II, it is not always observed, presumably due to the same effects we are trying to study. The BLR component of He II typically has a low EW and large Doppler width, so it is a relatively low-contrast feature. Moreover, when the NLR component is absent, any remaining He II emission appears significantly blueshifted and blended with (or part of) the C IV red shelf.[14] Second, because He II is a high-ionization line, an argument can be made that even the narrow component of this line arises, at least partially, in an outflow, as is suggested by the blueshifts of other high-ionization broad lines (e.g., Wills et al. 1993; Murray et al. 1995; Sulentic et al. 1995; Baskin & Laor 2005; Richards et al. 2011; Denney 2012).

[O II], on the other hand, is a forbidden narrow emission line, so it is emitted predominantly from the extended NLR that is not as susceptible to physical diversity due to kinematics and energetics deep within the potential of the BH that regulate the spectral properties of broad and possibly, to some degree, narrow recombination emission lines. [O II] can also be emitted throughout the host galaxy, which will also not be affected by the AGN environment and will lead to even more robust systemic redshift determinations. Shen et al. (2016) find a tight correspondence between the peak of the [O II] emission and stellar absorption lines for the lower-redshift subset of the SDSS-RM sample, with a systematic shift of only 8 km s^{-1} and an intrinsic scatter of 46 km s^{-1}. Consequently, the redshifts determined by [O II] for the present sample serve, in effect, as our control. While [O II] is the shortest-wavelength unblended forbidden emission line that is relatively strong and still present in quasar spectra for intermediate-to-high redshifts, it still falls

[14] An emission feature at $\sim$1600 Å that also varies in strength among quasars and has yet to be identified as uniquely due to any specific ionic species or blend (see, e.g., Laor et al. 1994; Marziani et al. 1996; Fine et al. 2010; Assef et al. 2011, for discussions and further references).

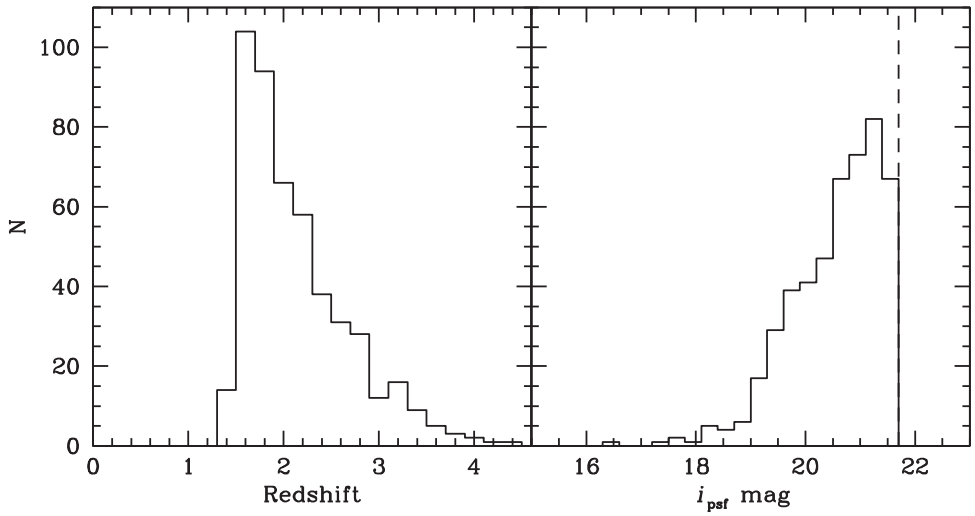

Figure 1. Distribution of redshifts and i_{psf} magnitudes for the sample of 482 $z > 1.46$ SDSS-RM quasars. The vertical dashed line in the right panel shows the magnitude limit for the SDSS-RM sample.

beyond the BOSS wavelength coverage for $z \gtrsim 1.78$, so only 154 of our 482 quasars have [O II] present in their spectra. Thus, while it is reliable, it is not very applicable to high-z quasars.

3.1. Direct Determination of the He II Redshift

Because of the spectroscopic diversity effects affecting the He II line across our sample, it is not as straight-forward to perform automated emission-line fitting (e.g., Shen et al. 2011) and still control for the optimal number and relative shift of fit components. Therefore, we first make a determination of the He II redshift by directly measuring the He II line center from the continuum-subtracted coadded spectra (i.e., not from functional-form fits to the He II line) based on interactively selected wavelength boundaries. We attempted to choose these boundaries at approximately the half maximum flux level on either side of the He II peak, selected by eye. We determine the He II line center from both the peak wavelength, by identifying the pixel within the interactively selected boundaries that contains the largest continuum-subtracted line flux, and the He II flux-weighted centroid measured within the same boundaries. Since the intrinsic strength of the He II line, especially the NLR component, varies between objects, the boundary selection is often quite subjective. In some objects, no He II line is visible at all, even for very high-S/N spectra, and in others, noise or absorption obscures the peak. In these cases, we also use other nearby emission features, such as the 1400 Å feature (a blend of Si IV and O IV]) and the O III] λ1663 lines, or even absorption lines, which have a high probability of being at or very near the systemic redshift (Nestor et al. 2008; Bowler et al. 2014; J. Allen & P. Hewett 2016, in preparation), to help inform the choice of the wavelength range that provides the most reasonable redshift through visual inspection under these circumstances. When we could discern no reasonable criteria for setting boundaries for a He II narrow component, the BOSS redshift was kept. Because of these difficulties, we assigned He II redshift quality (Q) flags to each object, defined by the following criteria:

> Very weak, or very broad, apparently blueshifted BLR component (compared to other features such as the 1400 Å feature and O III] λ1663 doublet) with no NLR component, or no obvious line;
> 1. Clean, narrow peak;
> 2. Noisy, but a relatively narrow peak is still clear;
> 3. Broader line, but a reliably determined peak;
> 4. Broader line, and the peak cannot be reliably attributed to a narrow component;
> 5. Noisy spectrum, where the peak/centroid is uncertain or possibly contaminated by noise or intervening absorption.

We take the redshift determinations from $Q = 1$, 2, and 3 objects to be relatively robust measurements of the systemic redshift, as a strong narrow component should not be significantly blueshifted, with $Q = 3$ the least robust due to the broader He II line. $Q = 4$, 5, and 0 are less robust due to data-related issues, intrinsic quasar properties, or both. Due to the overall subjectivity of these measurements, they are not to be taken as high-precision redshifts, but they nonetheless provide sufficient evidence to support our investigation. Coincidentally, the sample is roughly evenly divided, with 237 objects flagged with $Q = 1$, 2, or 3, and 245 objects flagged with $Q = 4$, 5, or 0. Figure 2 shows an example spectrum for each of the six quality categories. Choosing a "representative" example for each category that may be assigned for multiple reasons is somewhat complicated, so we provide additional comments on each example shown in Figure 2 to highlight some observed characteristics that were used to assign each Q category in these cases:

1. The Q1 example represents our cleanest category and shows a strong narrow He II with a clean peak.
2. The Q2 example shows an object where the clear, narrow He II component is contaminated by noise. Here, the large noise spike is due to a poor telluric absorption correction.
3. The Q3 example shows that while a He II peak is clearly identifiable in the spectrum, the flux selected as the "narrow" component is clearly broader than those examples from Q1, but is still narrow compared to an apparent very broad underlying He II component.
4. The Q4 example shows additional difficulties over Q3 objects in reliably identifying what may be a narrow component, since the whole line appears broader, sometimes asymmetric, as in this case, and often noisy.

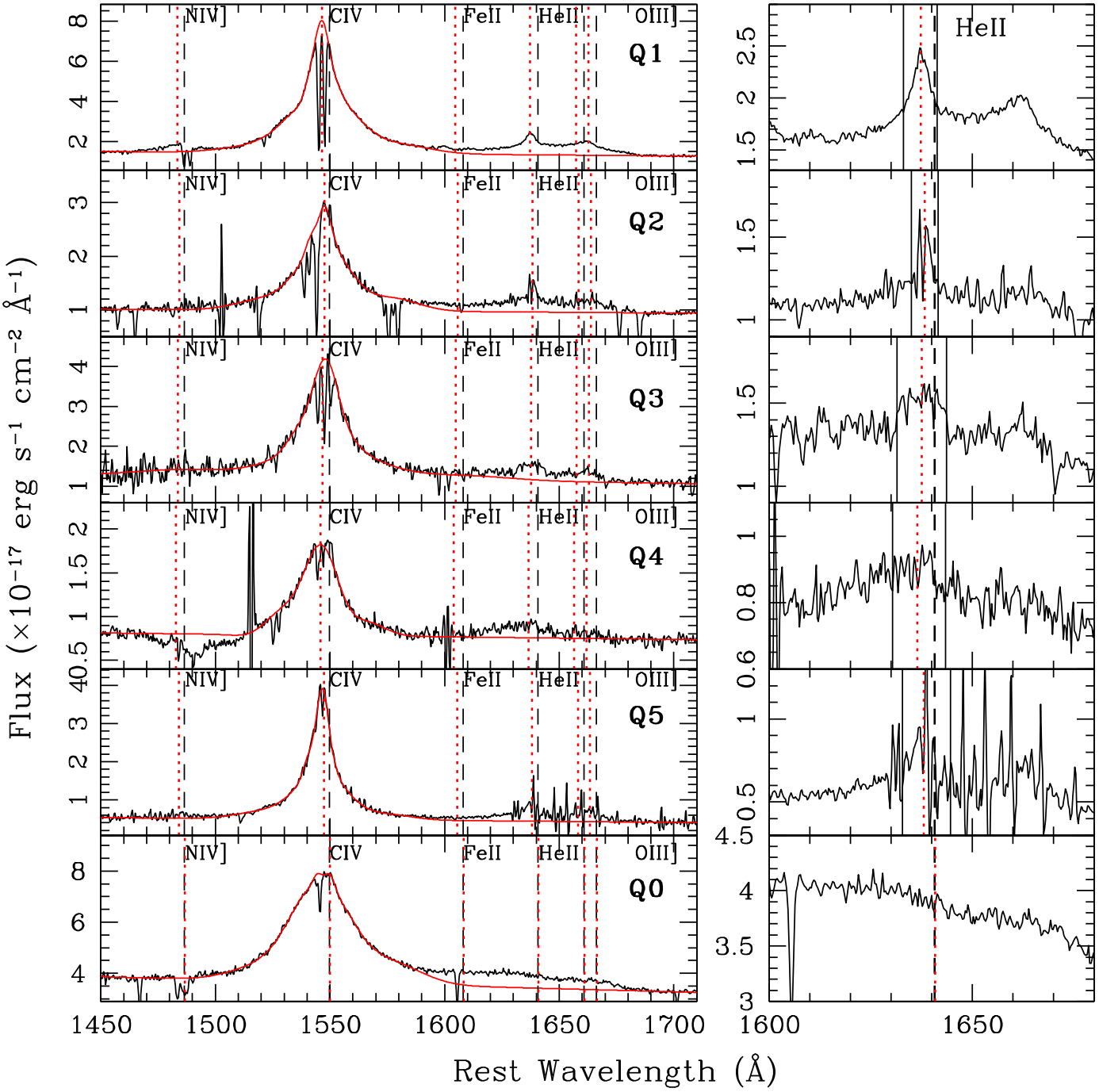

Figure 2. Examples of spectra for each of the six redshift quality categories described in Section 3.1. The left panels cover the C IV through O III] wavelength region, where the original spectrum is in black and the best-fit Gauss–Hermite polynomial model for the C IV profile from Denney et al. (2016) is in red. The quality (Q) category is given in the top right corner of each panel. The x-axis of each panel has been de-redshifted by the BOSS-pipeline redshift and the vertical black dashed lines show the expected location of the labeled emission lines based on the BOSS-pipeline redshift. The red dotted vertical lines show these expected locations based on our He II-based redshift. The right panels show the same object as each respective left panel, only zoomed-in to the He II emission line, with the expected positions of He II shown again by the same vertical lines as in the right panels. The solid black vertical lines show the "by-eye" roughly selected boundaries for calculating each He II centroid, which was used to determine the redshift. Note that the $Q = 0$ object does not have boundaries marked because no discernible He II was visible, and so we kept the BOSS-pipeline redshift for this object.

5. The Q5 example shows that the difficulty in measuring the He II line center reliably from objects in this category could be due to a mixture of causes, but these are dominated by noise and absorption, rather than intrinsic spectroscopic diversity. In this case, the He II line appears likely to have an intrinsically narrow, well-defined peak, but noise due to significant telluric-absorption-correction residuals in this $z = 3.44$ spectrum make it more difficult to isolate reliably.
6. The Q0 example shows clearly that some objects have no apparent narrow He II from which to inform the redshift, and we kept the original BOSS-pipeline redshift.

Once the peak and centroid were measured for all sources, we performed three analyses of these measurements to

determine which He II line center provides a more robust measure of the redshift and to test for significant systematic uncertainties due to the simplicity of our method:

1. We use 500 Monte Carlo (MC) realizations that resample the pixel-to-pixel flux density of each coadded spectrum with a Gaussian deviate based on the error spectrum. We then measure both the He II peak and centroid from the 500 resampled spectra using the same method as for the original coadded spectra, i.e., within the same He II boundaries, after subtracting the same linear continuum fit, the latter of which is robust to flux variations due to noise, as it is determined from the average flux measured over many resolution elements. We use the standard deviation of these 500 measurements to represent the statistical measurement uncertainty on the He II peak and centroid measurements for each object. The median uncertainty and scatter about the median, defined as half of the 16%–84% inter-percentile range (HIPR) that would correspond to 1σ if the distribution were Gaussian, for the full 482-quasar sample distribution are 3.7 and 3.3 km s^{-1} for the He II centroid, which are two orders of magnitude smaller than for the sample distribution of He II peak uncertainties: 400 km s^{-1} and 230 km s^{-1}, respectively. We find no statistically significant differences in the centroid uncertainties between the different quality flag categories. The median uncertainty in the He II peak wavelengths are ∼50% larger in the $Q = 4$, 5, and 0 subsample than in the $Q = 1$, 2, and 3 subsample (480 km s^{-1} versus 310 km s^{-1}, respectively), with the sample of Q1 objects having, on average, the smallest peak uncertainties, as expected.
2. We investigated possible systematics in the He II line center measurements due to the boundary selections with 1000 MC realizations that apply an independent, random deviate within the range $x \pm 2$ pixels, where x is the original, interactively chosen boundary, to both the He II upper and lower boundaries.[15] We recalculated the He II centroid and peak using these randomly deviated boundaries from each original, continuum-subtracted, coadded spectrum. We took the 68-percentile HIPR of each centroid and peak distribution of 1000 trials for each object to represent the uncertainty in each line center measure due to the boundary selections. As expected, with the exception of the a small fraction of outliers (∼5%), there is no change in the peak measurement when applying deviations to the boundaries. The median uncertainty in the centroid measurements for the full sample and for every subsample (i.e., combined $Q = 1$, 2, and 3 and $Q = 4$, 5, and 0, and every subsample of individual quality category) is 50 km s^{-1}, so there is no difference in the uncertainty due to the boundary selection across the spectroscopic diversity of He II.
3. We investigated the potential for a bias between the two measures of the He II line center—peak and centroid—by looking at the relative velocity difference between the two wavelengths with respect to the centroid, i.e., $\Delta V = (\lambda_{\rm peak} - \lambda_{\rm centroid})/\lambda_{\rm centroid} * c$. We calculate this difference for each of the 482 coadded sample spectra and determine the median and 68-percentile HIPR scatter for the full sample distribution, as well as that for the $Q = 1$, 2, 3 and $Q = 4$, 5, 0 subsamples. There is no difference, on average between the peak and centroid measurements in characterizing the location of the He II line center for the full sample: the median $\Delta V = -2$ km s^{-1}. The scatter for this distribution is 250 km s^{-1}. We find that there may be a mild systematic difference connected to the He II profile, as the median difference for the $Q = 1$, 2, 3 subsample is 30 km s^{-1}, while that for the $Q = 4$, 5, 0 subsample is -90 km s^{-1}. However, the HIPR scatter of these two subsample distributions is 160 km s^{-1} and 380 km s^{-1}, respectively, and given the size of statistical uncertainties in the peak measurements, the differences between the peak and centroid measurements of the line center with changing He II profile, i.e., quality subsample, are not statistically significant.

Given the significantly larger uncertainties associated with using the peak wavelength as the measure of the He II line center, in all that follows, any mention of "our He II-based redshifts" or the He II center refers to the He II flux-weighted centroid measurements, for which we assume a typical uncertainty of 50 km s^{-1}. Note that this uncertainty is associated with the precision with which a centroid can be calculated from user-defined regions and with the statistical uncertainty in this measurement due to spectral S/N. This uncertainty cannot address the accuracy with which this centroid represents the true center of the He II narrow component presumed to trace the quasar systemic redshift. As such, the overall uncertainties on our He II redshifts are likely larger than this, and so we further test the robustness of these measurements against independent measures of the redshift in the next section.

3.2. Automated PrepSpec He II and [O II] Redshifts

To form a control sample of redshifts based on a line not susceptible to spectroscopic diversity effects, we use the "PrepSpec" analysis of this sample. PrepSpec is a reverberation mapping spectral preparation and analysis software written by one of us (KH) and applied to the SDSS-RM Project sample (see Shen et al. 2015, for details). PrepSpec decomposes the time-resolved spectra into a mean spectrum plus continuum variations plus emission-line variations. The line variations are modeled as the product of an emission-line velocity profile times a light curve. All BLR, NLR, and host-galaxy emission lines visible in each spectrum are modeled as part of this process. The PrepSpec output includes measurements of the modeled emission-line centers, calculated using various metrics, and velocity offsets of these centers with respect to the input redshift values. While still dependent on automated modeling of the spectrum, this method provides an independent comparison for the He II line center, uncertainties on the measurements, and a homogeneous methodology for comparing to [O II]—our control, forbidden narrow line. We use the median flux center of the NLR model fit by PrepSpec to define the centers of the narrow He II and [O II] emission-lines, and the velocity offsets of these centers reported by PrepSpec are with respect to our He II-based redshifts, which we use as the input redshift. We focus only on the He II and [O II] λ3727 emission lines as a means to compare with our own He II-based

[15] Measurements are made in the observed frame spectrum, so 2 pixels corresponds to ∼70–150 km s^{-1} at the location of He II λ1640 over the redshifts probed by our sample, $1.46 < z < 4.33$.

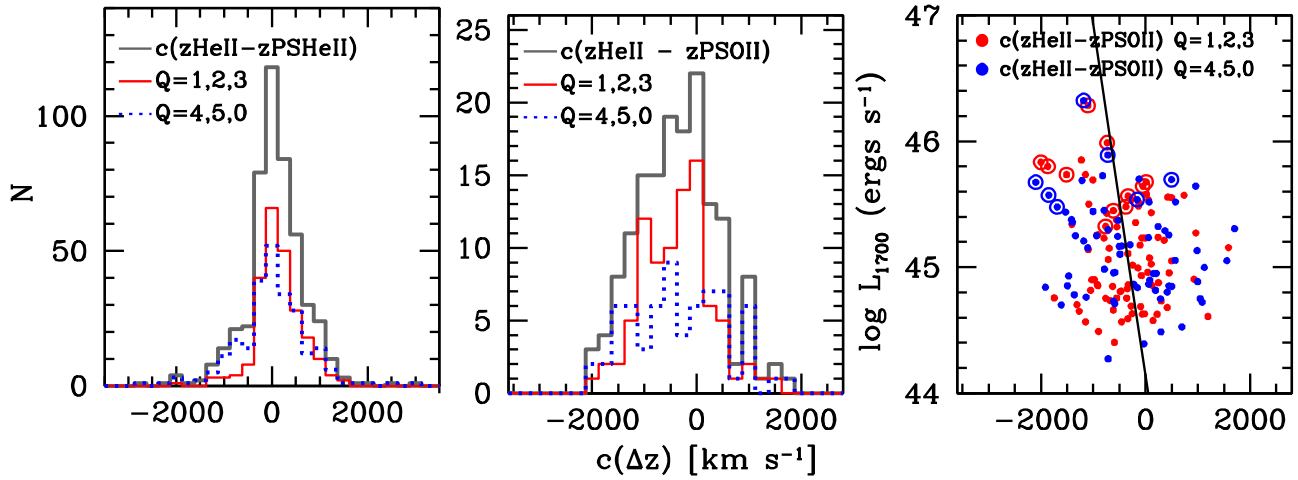

Figure 3. The left (middle) panel shows redshift differences between our He II redshifts and those determined for He II ([O II]) from an independent analysis using PrepSpec. The histogram colors are denoted in the legends. The right panel shows the luminosity-dependence of the velocity shifts between He II and [O II]. The solid black curve is a simple linear least-squares fit to the data. The points surrounded by larger open circles are sources that are also in the HW10 sample (see Section 4.3).

redshifts and to address the effects of quasar diversity on redshift (see Shen et al. 2016, for a comprehensive analysis of relative emission-line velocity shifts for this sample). Uncertainties in the measured line centers are determined from MC simulations. The median 1σ uncertainties in the PrepSpec He II and [O II] velocities are 481 km s^{-1} and 253 km s^{-1}, respectively.

3.3. C IV Blueshift Measurements

We use the analysis of the C IV emission-line region by Denney et al. (2016) to measure the C IV blueshift with respect to both the BOSS-pipeline redshifts and our He II-based redshifts. We utilize the C IV emission-line center measured from the centroid of the top 80% of the flux from Gauss–Hermite (GH) profile fits to the line. The uncertainties in the centroid measurements are estimated for each object from MC simulations that create 500 flux-resampled spectra on which the measurements are repeated. The median 1σ C IV centroid uncertainty for this full sample is 183 km s^{-1} (see Denney et al. 2016). To be consistent with a similar study presented by R11, we calculate our C IV blueshifts with respect to the estimated systemic redshift such that increasing blueshifts are larger, positive velocities, contrary to the usual convention.

4. DISCUSSION

4.1. Redshift Differences between Independent Analyses of the SDSS-RM Sample

Figure 3 and Table 1 show the differences between our He II-based redshifts and those inferred from PrepSpec for He II (left), for the full sample, and [O II] (middle), for the 154 objects that have this measurement. The PrepSpec He II redshifts are consistent with our simple, direct approach, given the uncertainties. The median difference between our He II centroid measurements and the PrepSpec He II line centers is 54 km s^{-1} which is only ∼10% of the median PrepSpec He II measurement uncertainty and consistent with that of our He II-based redshifts. Bootstrap MC simulations that draw 10,000 random samples from the distribution shown in the left panel of Figure 3, with no weighting for measurements drawn multiple times, estimate a 1σ (3σ) uncertainty in this median systematic shift of ±22 km s^{-1} (±62 km s^{-1}), further supporting the consistency between our rough, visually determined centroid-based He II line centers and those determined through PrepSpec fitting. This consistency further demonstrates that there is no statistically significant bias in our He II-based redshifts due to possible blueshifts of the underlying broad He II component, which was not removed in our simple approach but was in the PrepSpec fitting.

The comparison with [O II] (middle panel of Figure 3) predominantly shows a relatively large 68-percentile HIPR scatter of 780 km s^{-1}. A small systematic blueshift of He II relative to [O II] is evident, with the median velocity shift and 10,000 trial MC bootstrap 1σ (3σ) uncertainties of the distribution found to be 348 km s^{-1} $\pm$ 104 km s^{-1} (242 km s^{-1}). However, this systematic shift is not statistically significant, given the bootstrap uncertainties on the distribution median and the 1σ quadrature summed measurement uncertainties of our He II redshifts with the PrepSpec [O II] velocities offsets (260 km s^{-1}).

Since physical quasar diversity effects are expected to be imprinted on He II but not [O II], we also measured the systematic shift after splitting the sample by quality rating. We find somewhat larger, statistically significant, systematic shifts and more scatter for the more uncertain $Q = 4, 5, 0$ He II redshifts than for $Q = 1, 2, 3$ (see Table 1). Despite the contributions of noise to the $Q = 4, 5, 0$ distribution, this is also as expected if the primary source of the observed velocity shift is EV1 effects within the parameter space of the observed spectroscopic diversity of quasars. In this context, we expect the strength of narrow He II to anti-correlate with its the broad +narrow emission-line width and the velocity shift away from systemic. This physical effect is likely additionally exacerbated within the $Q = 4, 5, 0$ subsample by the uncertainty in our inability to isolate the He II narrow component when it is weak or absent. This leads to the combined effect of both larger systematic offset and larger scatter for these types of objects.

Shen et al. (2016) find similar but smaller relative velocity shifts, with a median He II shift of -175 km s^{-1}, i.e., blueward, with respect to [O II] using yet another independent method for fitting the emission lines in the coadded spectra of the SDSS-RM sample. Shen et al. (2016) use a slightly different sample than ours, including only 134 objects with both He II and [O II] due to a combination of spectral-fitting redshift and/or

Table 1
Quasar Redshift Differences and C IV Blueshifts

Distribution Property (1)	Sub-sample Description (2)	Number of Obj. (3)	Median Sample[a] S/N (4)	Distribution Median[b] (5)	Distribution HIPR[b] (6)	Distribution Mean[b] (7)	Distribution Std. Dev.[b] (8)
Redshift Differences:							
BOSS–He II	All	482	25.7	1080	1605	1057	2459
BOSS–He II	$Q = 1, 2, 3$	237	23	1320	1230	1366	1928
BOSS–He II	$Q = 4, 5, 0$	245	29.7	690	2085	758	2854
BOSS–HW10	HW10+SDSSRM	47	61.5	−386	1781	−618	2112
BOSS–He II	HW10+SDSSRM	47	61.5	990	1755	948	2782
HW10–He II	HW10+SDSSRM	47	61.5	1500	1898	1566	2644
HW10–He II; $Q = 1, 2, 3$	HW10+SDSSRM	17	81.1	1500	1641	1310	1687
HW10–He II; $Q = 4, 5, 0$	HW10+SDSSRM	30	59.7	1319	2231	1711	3076
He II–PSHe II	All	482	25.7	54	475	66	617
He II–PSHe II	$Q = 1, 2, 3$	237	23	98	402	130	472
He II–PSHe II	$Q = 4, 5, 0$	245	29.7	5	620	3	726
He II–PS[O II]	SDSSRM w/[O II]	154	24.7	−348	780	−354	775
He II–PS[O II]; $Q = 1, 2, 3$	SDSSRM w/[O II]	87	23.2	−339	643	−377	667
He II–PS[O II]; $Q = 4, 5, 0$	SDSSRM w/[O II]	67	25.1	−455	963	−325	901
C IV Blueshifts:							
BOSS-based z	All	482	25.7	1258	664	1526	1874
BOSS-based z	$Q = 1, 2, 3$	237	23	1217	615	1394	1740
BOSS-based z	$Q = 4, 5, 0$	245	29.7	1301	729	1652	1989
He II-based z	All	482	25.7	26	706	469	1899
He II-based z	$Q = 1, 2, 3$	237	23	−118	362	29	1323
He II-based z	$Q = 4, 5, 0$	245	29.7	459	1111	895	2247

Notes.
[a] The median S/N is based on the distributions of coadded spectra. The S/N is measured per angstrom, integrated over an emission-line-free continuum window, ΔW, covering many resolution elements near restframe 1700 Å.
[b] The median, HIPR, mean, and standard deviation (Std. Dev.) values are in units of km s^{-1}.

wavelength limits and the reliability of the automated fitting process in identifying and fitting the lines in cases where they are weak. This may contribute to the relatively smaller systematic shifts and scatter they find compared to the present results.

In addition, Shen et al. (2016) find luminosity trends in relative line shifts in the SDSS-RM sample, or equivalently, redshift determinations based on cross-correlation with different emission lines, consistent with other work (HW10; R11; Shen et al. 2011; Shen & Liu 2012). HW10 discuss the systematic effects in cross-correlation redshift determination between lines as due to SED effects—for example, the differing line ratios within the C III] blend. These are most certainly related to the EV1, or physical quasar diversity, effects we are interested in here. HW10 do not directly take these effects into account, although they do apply a correction as a function of quasar luminosity that is arguably related, but there is much scatter. We see from the right panel of Figure 3 that there is a weak correlation as a function of luminosity for our He II–[O II] velocity shift measurements, consistent with the results of Shen et al. (2016). However, there is significant scatter about this weak correlation, arguably driven by the lack of scatter toward positive shifts at high luminosity, rather than a consistent trend across the full luminosity range. Nonetheless, this trend goes in the direction expected from the SED and EV1 effects, where the highest luminosity, highest accretion-rate sources are more likely to have signatures of quasar outflows in their spectra (see also discussions by, e.g., R11 and references therein).

4.2. He II Redshifts Compared to BOSS Pipeline Redshifts

We investigate the possibility for biases in the BOSS-pipeline redshifts due to quasar diversity using our He II redshifts described in Section 3.1. Table 1 quantifies the redshift differences we find between BOSS-pipeline and He II-based redshifts, which are shown in Figure 4. We look separately at the full sample as well as the "more" ($Q = 1, 2, 3$) and "less" ($Q = 4, 5, 0$) reliable subsamples. The peak of the full sample distribution is broad, but generally, we find a median shift in the BOSS redshifts of 1080 km s^{-1} relative to those based on He II, with a 1σ (3σ) uncertainty on the median from 10,000 bootstrap trials of 90 km s^{-1} (225 km s^{-1}). This systematic difference is significantly larger (greater than a factor of three) than the median shift between He II and [O II] that can be explained by spectroscopic diversity effects in the He II redshifts.

The bottom three panels of Figure 4 show how the redshift differences depend on redshift, coadded continuum spectral S/N, and luminosity. By comparing the running mean curves, we find that the BOSS–He II redshift differences increase by a factor of ∼2 for quasars with $z > 2.7$, probably because this corresponds to the redshift where Mg II exits the BOSS spectral range (shown by the vertical dashed line). There appears to be a larger bias for systems with low S/N. At face value, this could follow with general effects of data quality on measurements of emission-line properties (Denney et al. 2016). However, the He II centroid uncertainties estimated in Section 3.1 show that the centroid is very stable to statistical noise fluctuations in the spectral flux. To facilitate an alternative interpretation, we have indicated objects with coadded S/N > 50 with green circles in

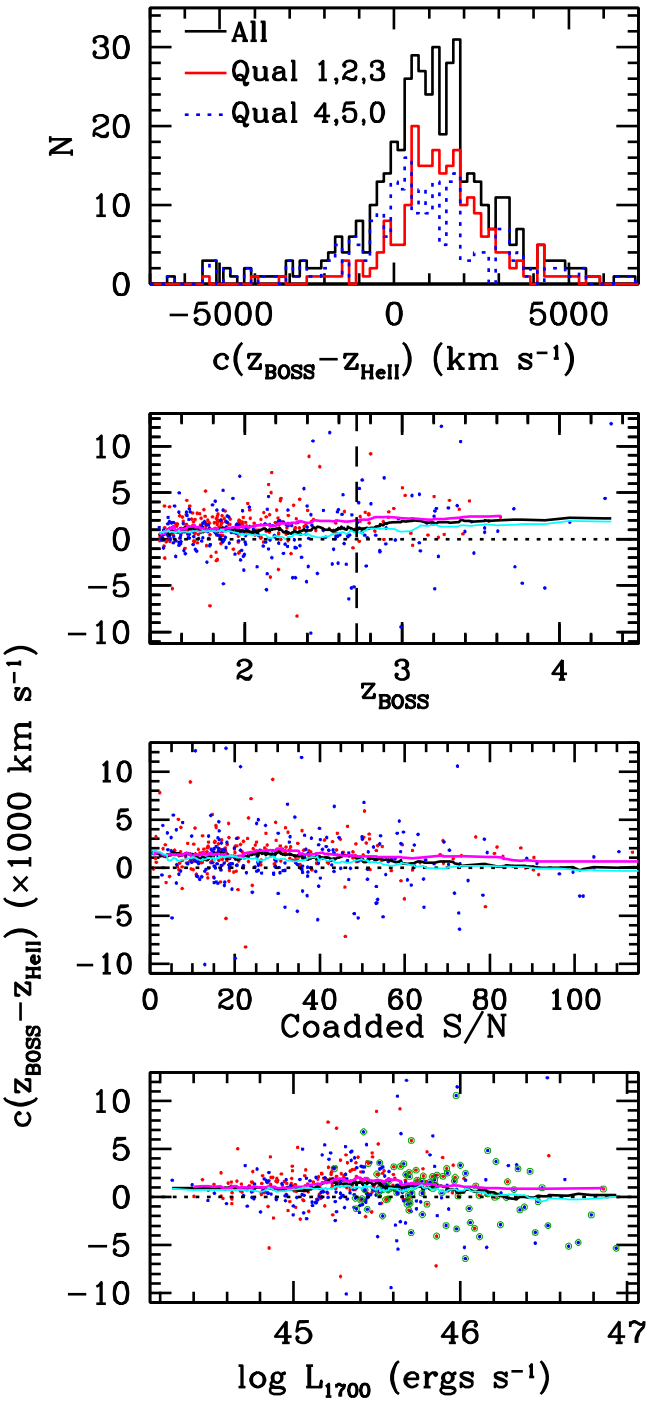

Figure 4. The difference between BOSS-pipeline and He II redshifts. The top panel compares the BOSS-pipeline redshifts to those from the He II λ 1640 line centroid measured from the coadded spectra; black represents the full sample, and the "more" ($Q = 1, 2, 3$) and "less" ($Q = 4, 5, 0$) reliable subsamples (see Section 3.1) are shown by the red solid and blue dotted histograms, respectively. The bottom three panels, ordered highest to lowest, show the redshift differences of the $Q = 1, 2, 3$ objects in red and the $Q = 4, 5, 0$ objects in blue as a function of (i) BOSS redshift, (ii) median single-epoch S/N, and (iii) luminosity. The solid curves show a 51-pt running mean of the redshift differences for the full (black), $Q = 1, 2, 3$ (magenta), and $Q = 4, 5, 0$ (cyan) samples. The horizontal black dotted lines are a reference for equal BOSS and He II redshifts. The vertical dashed line in the highest of the three panels shows where the Mg II emission line redshifts out of the BOSS wavelength range. Green circles in the bottom panel indicate objects with coadded S/N > 50.

the bottom panel. All are found to have relatively higher luminosities, as expected. While these high-S/N objects have relatively low BOSS–He II redshift differences, we see from the bottom panel that nearly all of the highest-luminosity objects—where the running means show the redshift differences are also the smallest—have high S/N. Furthermore, there are ∼50% more $Q = 4, 5, 0$ objects than $Q = 1, 2, 3$ objects in this high-S/N group, and the former subsample exhibits smaller redshift differences, overall, but the smallest differences at the highest luminosities. The dependence of the BOSS–He II redshift differences with S/N is thus a result of the dependence with luminosity—and spectroscopic quasar diversity effects—within a flux-limited sample. These quasar-diversity-dependent trends with luminosity remain present in the BOSS-pipeline redshifts despite the improvements we expected by using PCA analysis over strict emission-line cross-correlation with a composite spectrum.

We find the smallest BOSS–He II redshift differences, on average, at the highest luminosities, $\log L_{1700}(\mathrm{erg\ s^{-1}}) > 46$, as indicated by the running mean curves in the bottom panel of Figure 4. However, extrapolation in Figure 3 suggests that objects with these high luminosities have the largest deviations between He II and [O II]—up to ∼2000 km s^{-1}—presumably owing to EV1 quasar diversity effects. The number statistics is comparatively poor in this regime, but the bottom panel of Figure 4 demonstrates that most high-luminosity objects are in the $Q = 4, 5, 0$ subsample (blue points; cyan curve) and even exhibit a negative redshift difference, on average, at L_{1700} (ergs s^{-1}) ∼ 46.5, while the $Q = 1, 2, 3$ objects (red points; magenta curve) remain offset in redshift by ∼1000 km s^{-1}. Our interpretation for this high-luminosity trend is that *both* the BOSS and the $Q = 4, 5, 0$ He II redshifts are biased (i.e., underestimating the systemic quasar redshift). High-luminosity objects tend, through EV1 effects, to have weak He II, and thus He II is a poor redshift indicator for these quasars. Nonetheless, our He II method attempted, where possible, to use other lower-EW features or absorption lines in these cases to inform the redshift, which is an advantage not currently available to the BOSS pipeline. So the BOSS pipeline may be underestimating the systemic redshift even more than our He II method, thus explaining the negative redshift differences.

At lower luminosities, we find differences between He II- and BOSS-pipeline redshifts of ∼1000 km s^{-1}, or more, for both subsamples. Recall that the $Q = 4, 5, 0$ subsample encompasses not only weak or broad He II profiles, but also noisy profiles with ambiguous peaks. This subsample is more likely to be dominated by the noisy, narrow-He II objects at these low luminosities, thus explaining the consistent redshift differences for the two subsamples. These lower luminosity sources have He II redshifts consistent with those from [O II] and are thus likely to be probing the systemic redshift. The largest observed redshift difference is at intermediate luminosities in both subsamples and is likely consistent with the increased bias of BOSS-pipeline redshifts experienced when Mg II shifts out of the observed spectral range.

These results suggest that both high-luminosity and low-luminosity quasars are biased in opposite senses: BOSS redshifts of high-luminosity quasars are underestimated, while those of low-luminosity quasars are overestimated. This

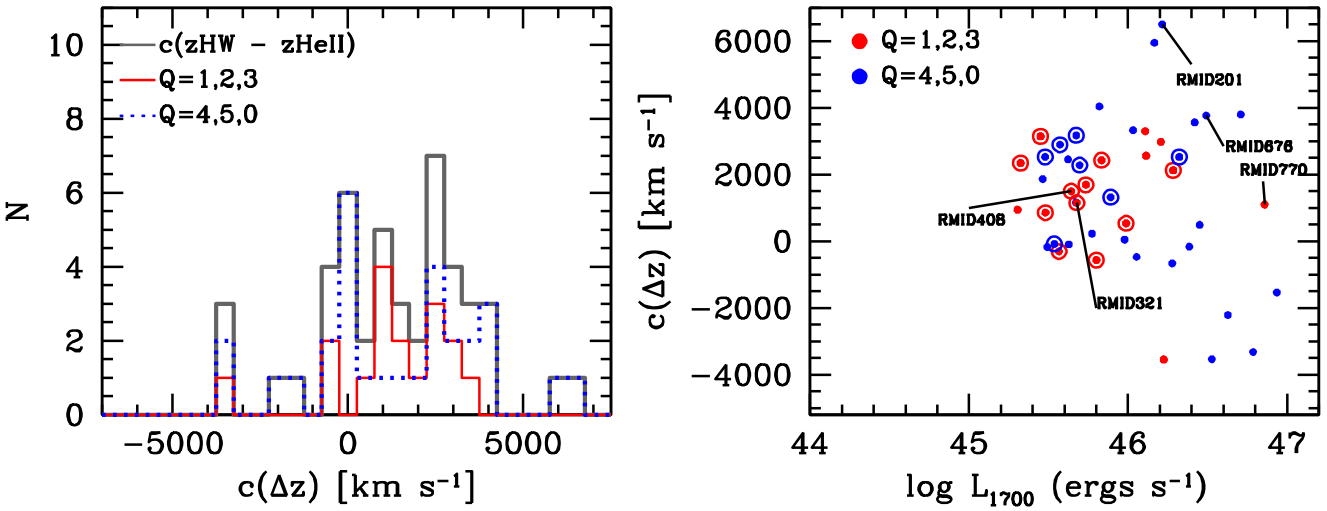

Figure 5. Left: same as the top panel of Figure 4 but between our He II redshifts and the HW10 redshifts for the shared sample of 47 objects. Right: same as the right panel of Figure 3 but for redshift differences between our He II redshifts and the HW10 redshifts. The points surrounded by larger open circles are sources that also have [O II] measurements. Selected objects discussed in Section 4.3 are individually identified.

effectively compresses the redshift–luminosity plane, or the parameter space of any other measured or physical properties with similar dependencies. In other words, cross-correlation redshifts have an "averaging" bias in not accounting for the dependence of quasar line shifts on luminosity (see HW10) or some more physical underlying source. This was in some sense done by design in SDSS-pipeline redshifts, where the Vanden Berk et al. (2001) template was created with C IV at 1546 Å, so that contributing quasars that were noted to have a range in C IV peak wavelengths spanned the template wavelength about ± 1000 km s^{-1}, rather than a template with C IV at the expected 1549 Å, with objects showing shifts in the range $\sim$0–2000 km s^{-1} (G. T. Richards 2016, private communication). The best explanation we can determine for this effect remaining so large in BOSS-pipeline redshifts is the implicit dependence of the BOSS-pipeline redshifts on cross-correlation redshifts: the PCA training sample redshifts are still based on a comparison to a composite spectrum, despite the improvements afforded by PCA.

4.3. A Comparison to HW10 Redshifts

As discussed previously, HW10 attempted to mitigate quasar-diversity biases in SDSS-pipeline redshifts by applying a luminosity correction. In Figure 5 we compare the He II redshifts to HW10 redshifts[16] for the 47 quasars (17 with $Q =$ 1, 2, 3) we have in common with HW10. The left panel of Figure 5 and statistics in Table 1 show a larger shift between our He II redshifts and HW10 redshifts than the small differences we measured between He II and [O II]. This is, at first glance, surprising, since HW10 made corrections to the SDSS redshifts for the luminosity-dependent biases.

One interpretation of these differences is that there are still spectroscopic diversity systematics in the HW10 redshifts, despite the improvements and corrections they employ. They do still make use of cross-correlation with template spectra and so may still be susceptible to averaging across the diversity to form their composite spectra. Alternatively, we may simply be "unlucky" in our overlap sample. Admittedly, the number statistics of our comparison are small and the scatter is large. From a quasar physics standpoint, however, the SDSS spectroscopic flux limit is shallower than that of BOSS and SDSS-RM. So the overlap of HW10 sources with our SDSS-RM sample is biased to bright AGNs only. This implies the distribution of overlap with our SDSS-RM sample is not unbiased. Indeed, the open circles in the right panel of Figure 5 show that the 18 objects in our overlap sample with HW10 that also have [O II] redshifts are not distributed uniformly and, instead, exhibit larger than average shifts between He II and the systemic redshift (assumed from [O II] measurements).

With this biased sample-overlap, we cannot make an objective and comprehensive investigation into the degree to which HW10 redshifts effectively correct for EV1/SED effects, and/or whether they may still be susceptible to spectroscopic diversity biases. However, we try to gain a small amount of additional insight by looking at the 36 of the 47 objects in the SDSSRM–HW10 overlap sample that have Mg II present in the spectrum (shown in Figure 6). Of these, 30 of the HW10 redshifts are based on Mg II cross-correlation, which is generally taken to be the most reliable broad line for determining redshifts for $0.8 < z < 2.8$. For example, within the SDSS-RM sample, Shen et al. (2016) find only a small systematic shift, -57 km s^{-1}, on average, between the location of the Mg II peak and the Ca II stellar absorption features, with no luminosity dependence. There are 15 objects of this subsample that have $Q = 1$, 2, 3. From inspection of the observed Mg II doublet peaks in Figure 6 relative to the predictions from the He II-based redshift (solid lines), BOSS redshift (dotted lines), and HW10 redshift (dashed lines), there is not an obvious, uniform explanation for the redshift differences.

For the three objects (RMID 321, RMID408, and RMID770) with $Q = 1$ (for which He II redshifts are the most robust), we find that the He II redshift more accurately predicts the peaks of the Mg II doublet than the BOSS-pipeline or HW10 methods. All three of these objects display a shift between the He II and HW10 redshifts of $\sim$1000 km s^{-1}, consistent with the average He II–BOSS redshift difference. Yet, RMID321 and RMID408, two of the three objects that also have [O II] measurements, show a relative shift between [O II] and He II of only 11 km s^{-1} and -52 km s^{-1}, respectively. At least in these cases, this

[16] Available from http://das.sdss.org/va/Hewett_Wild_dr7qso_newz/.

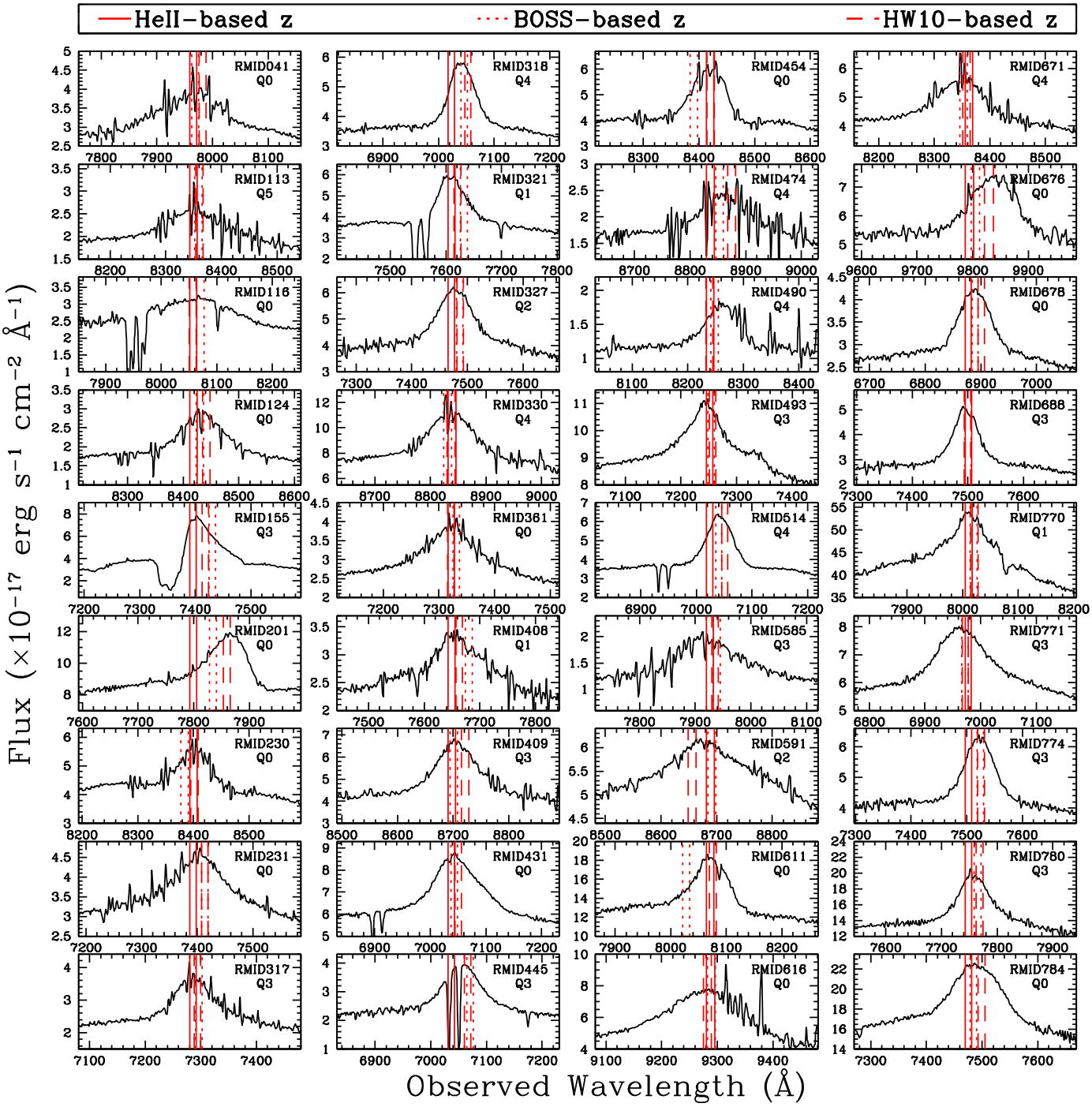

Figure 6. Mg II emission lines for the 36 SDSS-RM sample objects that also overlap with the HW10 sample. Vertical lines show the expected location of the Mg II doublet peaks given the redshift estimate provided by each method shown in the legend at the top. RMID and He II-redshift quality rating are shown in the top right corner of each panel. All spectra are shown in the observed frame because of the uncertainty of which redshift is correct.

provides strong evidence that the He II redshift for these objects is trustworthy.

Consistent with the large scatter in the left panel of Figure 5, there is a lot of inconsistency in the Mg II peak-prediction accuracy of the $Q = 2$ and $Q = 3$ He II redshifts: in some objects, the He II-based redshift is better (e.g., RMID155), while for others (e.g., RMID774), it makes a much worse prediction than BOSS or HW10. Sometimes the HW10 redshift is clearly superior to the BOSS or He II estimate, such as for RMID201 and RMID676, both $Q = 0$ cases where He II is frequently asymmetric and is often blueshifted with respect to [O II], and/or no discernible narrow He II emission line is present. These cases highlight the clear improvement in redshifts offered by the luminosity (i.e., quasar diversity) corrections of HW10 over the SDSS or BOSS pipeline.

There are two other considerations when comparing results with Mg II, which is likely the best UV broad line to use for redshifts. First, even Mg II is sometimes blueshifted with respect to Hβ and [O III] $\lambda\lambda$4959, 5007 (e.g., Marziani et al. 2013; Plotkin et al. 2015). Such objects tend to be the same that are argued to have high accretion rates, high luminosity, blueshifts, and low-EW, high ionization lines (e.g.,

Sulentic et al. 2007; Richards et al. 2011; Luo et al. 2015). These objects are possibly also related to so-called weak-line quasars that also may have characteristically weak or absorbed X-ray properties and are suggested to lie at the extreme end of this parameter space (e.g., Luo et al. 2015; Plotkin et al. 2015). Furthermore, Mg II likely has little or no emission contribution from the NLR because of the photoionization physics regulating this transition. As such, diversity in BLR kinematics between objects will affect redshifts based on the Mg II peak compared to redshifts determined from narrow emission lines or host-galaxy stellar absorption lines. This is likely a cause of scatter in the peak shifts between Mg II and [O II] found by Shen et al. (2016) and others. Second, the Mg II doublet *ratio* depends on the physical conditions of the BLR. While the doublet is often not fully resolved due to moderate spectral resolution or because of the large BLR velocities, the line peak can still shift among differing physical environments that allow the ratio to vary between 1:1 and 2:1. Interpreting cross-correlation results therefore becomes non-trivial, and such effects will also affect the characteristics of the PCA training set or template spectrum. Clearly, this is a difficult and multi-faceted problem. While Mg II is certainly better than other UV quasar emission lines that exhibit more blending or stronger EV1/quasar diversity effects, Mg II will still exhibit diversity due to the physical environment of the nucleus.

4.4. Implications from BOSS Redshift Biases

The implications that BOSS quasar redshifts are biased are far-reaching. The SDSS collaboration has worked hard to acquire, reduce, and distribute this rich database to the community, as well as understand the systematics present within it, and the results of their efforts are evidenced in the vast literature based on this survey. Many SDSS/BOSS-based results, such as that of the main goal of BOSS—measuring baryonic acoustic oscillations (BAO) from the Lyα forest—do not require redshifts of precision greater than the bias found here. Thus these results and many others remain unaffected by the current results. However, the same is not necessarily true of some other studies, so it is important to understand the effect these biases may have on various current and future science investigations. For example, the results of the future eBOSS survey will be sensitive to this bias, as it will utilize, in addition to other redshift sources, a sample of >500,000 quasars to measure BAO distances over the range $0.9 < z < 2.2$ (Dawson et al. 2016). We draw attention to a few additional examples in the sections that follow.

4.4.1. C IV Blueshifts

A particular problem of special interested to us associated with accurate quasar redshift estimates is whether BH masses can be well-estimated using the C IV emission line. In particular, the apparent blueshifts in the C IV line have been used as evidence that the C IV velocity widths are indicative of non-virial motions and therefore ill-suited for virial BH mass calculations (see also Baskin & Laor 2005; Netzer et al. 2007; Sulentic et al. 2007; Shen et al. 2008; Shen & Liu 2012). However, since radiation-driven winds generally have velocities comparable to the BH escape velocity (Cassinelli & Castor 1973), they might still be quite reasonable virial estimates in this scenario. In any case, the inference of significant and/or generally ubiquitous blueshifts in C IV emission depends on the reliability of the redshifts.

Many of the C IV blueshifts previously inferred for SDSS quasars by R11 and others will be similarly biased if the quasar redshift determinations are unreliable. We still find evidence from our C IV peak flux-weighted centroids (using $f > 0.8f_{\rm peak}$) that the C IV peak exhibits blueshifts (as do other high-ionization broad lines, including He II), *but only in some quasars*. This is demonstrated in Figure 7, where the top panels show the measured C IV centroid blueshifts based on the BOSS-pipeline redshifts (top left) and our He II-based redshifts (top right). We find different trends for $Q = 1, 2, 3$ sources as for $Q = 4, 5, 0$ sources. The distinction between these subsamples, while technically set by our ability to reliably determine a He II-based redshift, is, as argued above, related to the differences in the spectroscopic, and presumably physical, properties of these sources.

Objects with strong (or relatively stronger), narrow He II emission components (typically $Q = 1$, 2, and 3) do not have systematically blueshifted C IV emission, while objects without this narrow component can show very large C IV blueshifts that are likely caused by SED effects, such as radiation line-driven outflows (see, e.g., R11; Denney 2012, and references therein for further discussion). However, Figure 7 and the discussions above provide evidence that BOSS-pipeline-based redshifts are even more biased than redshifts based on He II, even considering the shortcomings of using this line. The most likely explanation for these biases is due to the measurement of redshifts from cross-correlation with template spectra that are formed from a sample that covers the spectroscopic diversity parameter space of quasars. This complicates (i) analyses that try to understand the physical parameter space inferred from these spectroscopic differences using C IV diagnostics, or (ii) any study that requires reliable redshifts as a means to interpret emission- or absorption-line velocity shifts in quasar spectra (e.g., Khare et al. 2014).

Evidence for the averaging effect discussed in Section 1—likely due to the ultimate dependence of the BOSS-pipeline redshifts on an average composite spectrum—is shown in the top left panel of Figure 7. The distribution of C IV blueshifts for $Q = 1$, 2, and 3 redshifts is co-spatial with the $Q = 4$, 5, and 0 distribution, and all objects are driven to an "average" C IV blueshift, likely coincident with that imposed by a bias intrinsic in the redshifts of the PCA training set of quasar spectra. On the other hand, using the He II-based redshifts, we still find C IV blueshifts (some very large), but the lower limit is consistent with no blueshift, within the precision of our measurements. Importantly, the overall dynamic range of C IV blueshifts is much larger now that the averaging bias has been corrected.

Similar evidence is also seen by investigating the C IV blueshift–EW parameter space used by R11 (bottom panels of Figure 7). R11 argue that this observational parameter space traces physical quasar properties with respect to the prevalence of disk-winds (due to differences in mass accretion rate). Our results are consistent with this picture, but we argue that the effect of disk winds on C IV is not as ubiquitous as that indicated by R11 at a significance level that would statistically bias BH mass estimates, i.e., with a systematic blueshift larger than the typical velocity width measurement uncertainties. Despite the use of the improved HW10 redshifts by R11, the most likely explanation for the difference between their C IV blueshift results and what we find here is a remaining bias

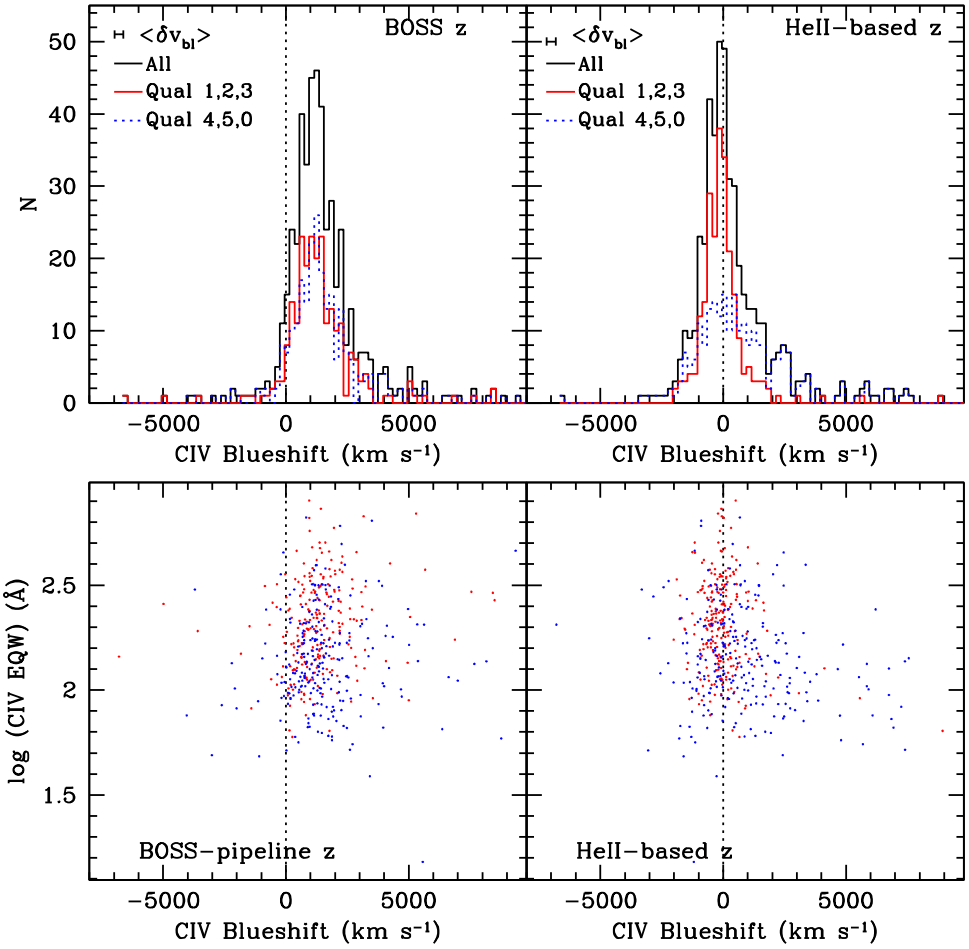

Figure 7. C IV blueshifts inferred from different redshift determinations. The top panels show implied C IV line centroid blueshifts based on the BOSS redshifts (left) and He II-based redshifts (right). Colors are the same as the top panel of Figure 4. The median C IV centroid uncertainty of 183 km s^{-1} is represented by the $\langle \delta v_{\rm bl} \rangle$ error bar in the top corner. Here, we use the same convention as R11 that larger blueshifts are indicated by larger positive velocities. The bottom panels show the same C IV blueshifts where the points follow the same color coding as the histograms in the top panels, but are shown with respect to the C IV line equivalent width, which are taken from Denney et al. (2016).

because of the shallower flux-limited SDSS sample compared to what we probe with SDSS-RM. Our analysis here suggests that because the HW10 correction is suboptimal for the lowest accretion-rate region of quasar parameter space, the results of R11 do not accurately describe C IV blueshift trends across the full range of quasar properties.

The left panels of Figure 7 show that both subsamples—those with stronger, narrow He II lines (red) and those without (blue)—occupy the same part of this parameter space when basing the C IV blueshifts on BOSS-pipeline redshifts but become separated when the C IV blueshift is measured with respect to the He II redshifts. This further supports the physical picture that is presented by R11: quasars with significant C IV blueshifts are likely those with strong disk winds. However, the C IV blueshift—suggestive of a dominant disk wind—is not ubiquitous among the quasar population; a number of quasars show, on average, *no* systematic blueshift within our measurement uncertainties. These are predominantly objects with strong low-velocity (narrow) He II and C IV emission-line cores.

One might argue that the disappearance of a systematic C IV blueshift for a portion of our targets when using He II-based redshifts simply indicates that He II and C IV share similar blueshifts and that the BOSS redshifts are not biased. However, note that objects with the smallest C IV blueshift are also those with He II emission clearly attributable to an NLR emission that show little to no velocity shift with respect to [O II] or Mg II (e.g., RMID321 and RMID408), so this interpretation is unlikely for this population of quasars. The *broad* He II component (the only visible component for many objects) shows similar shifts as the other high-ionization lines, so broad He II likely does trace C IV. As such, the results shown in Figure 7 are still not fully unbiased. Our interpretation of the results is that instead, given accurate, unbiased redshifts, we might expect the bottom right panel of Figure 7 to be adjusted as follows. To account for the small observed velocity shifts between He II and [O II] of 339 km s^{-1} (likely attributable mainly to the $Q = 2$ and 3 objects with broader "narrow" He II lines), the distribution of $Q = 1$, 2, 3 sources would likely be somewhat broader with a possible mean C IV blueshift of a couple of hundred km s^{-1} (as opposed to the current observed median C IV blueshift of -118 km s^{-1}, i.e., a redshifted C IV peak; see Table 1). Even correcting for this [O II] shift, we would still expect the lower limit of C IV blueshifts to be at ∼zero. Next, to account for the bias in objects with unreliable He II redshifts due to the lack of a visible He II narrow component—mostly $Q = 4$, 5, 0 quasars—we would expect this distribution of objects to exhibit a higher median C IV

blueshift than observed. If our He II centroid measurements were biased by selecting broad He II emission, blueshifted similarly as C IV, for high accretion-rate sources with strong winds and no narrow He II, the He II redshift is likely biased low, thus underestimating the true C IV blueshift.

4.4.2. The Quasar Nucleus, Environment, and Black Hole Mass

Some studies may be largely unaffected by these redshift biases, e.g., the Lyα forest BAO measurements that rely only on the relative redshifts of Lyα absorption systems. However, it is conceivable that some studies that rely on quasar redshifts to set the zero point for relative velocity shifts, such as to investigate associated and intervening absorption, may incur systematic biases even beyond those explainable to first order by the BOSS redshift biases described in this work.

Our He II-based redshift analysis suggests that the reliability, i.e., degree of bias, of current high-z quasar redshifts can be connected to the intrinsic, physical differences in the quasar physics, e.g., possibly the nuclear structure and/or SED, likely related to accretion rate (see, e.g., Leighly 2004; Baskin et al. 2013; Luo et al. 2015) imprinted as spectroscopic diversity. If galaxy evolution is predicated on a not yet well-understood relationship between the nuclear activity and the host galaxy, then the connection between the redshift biases and physics of the nucleus could extend to a connection with the quasar environment. This implies that for a random population of quasar spectra, systematic biases in the redshifts due to the physical properties *within* quasars may be correlated with the physical properties inferred from the absorption lines, presumably arising *outside* the nucleus but still connected within the framework of blackhole–galaxy co-evolution. Thus, the quasar redshift biases may not statistically "average out", even for large absorption-line studies. For example, Nestor et al. (2008) reported a mysterious over-density of C IV narrow absorption lines blueshifted by $\sim$2000 km s^{-1} with respect to the apparent systemic redshift in a sample of SDSS quasars. Bowler et al. (2014) also see this over-density, even after updating the quasar redshifts with the HW10 database. However, a recent re-analysis of this sample makes similar, though through a completely independent method, corrections to the redshifts to account for the same quasar diversity effects we draw attention to in this work and shows that the over-density was, in fact, an artifact of redshift biases (J. Allen & P. Hewett 2016, in preparation).

On the other hand, correlations of the redshift biases with physical properties of the quasars can be used to further enlighten studies of the nuclear physics, BH accretion, and on a larger scale, galaxy evolution. Indications of this connection available in the literature have been cited throughout this work but are largely limited to relatively local and/or small samples with well-defined properties, such as redshift. Future work to secure more accurate systemic quasar redshifts will increase our ability to learn about the physical implications for the intrinsic shifts in quasar emission lines and how these shifts are connected to, e.g., the intrinsic structure and evolution of the quasar and its environment. For instance, the correlation seen here and elsewhere between the blueshifts/asymmetries in the BLR component of high-ionization lines like C IV and He II and the presence and/or strength of NLR components presents the possibility that the structure of the NLR and BLR may be intrinsically connected. Given the large spatial separation between these two regions, the observed connection may be one of energetics, e.g., the structure and presence of outflows and winds from the nucleus, or one of evolution, e.g., the mechanism by which gas reaches the nucleus. Additional connections between these emission line properties and the SED hint at the accretion rate and the energetics being important in understanding the observed connections, but future work is needed in this area, and additional speculation is outside the scope of this work.

The result described in the previous section that a relatively well-defined sample of quasars, i.e., those with strong narrow components, does not exhibit C IV blueshifts, also has implications for C IV-based BH mass estimates. The reliability of C IV single-epoch scaling relationship-based BH masses has been called into question partially because of the presumed ubiquitous presence of these blueshifts and their being attributed to non-virial motions in the BLR. If instead, C IV blueshifts are not ubiquitous, and redshifts are reliably determined, carefully chosen samples can largely avoid objects observed to exhibit presumed non-virial BLR motions much larger than the uncertainties in the line width measurements used for estimating the BH masses. This could help improve the reliability of BH mass estimates based on current calibrations. On the other hand, an additional problem with current single-epoch C IV masses is one of sample conflict: the sample with which the C IV single-epoch mass scaling relationship is calibrated is limited by the availability of C IV reverberation mapping results to low redshift, relatively low-luminosity and low-accretion-rate sources (Vestergaard & Peterson 2006; Park et al. 2013), which is not representative of the typical sample to which it is applied (high-redshift, high-luminosity, likely high-accretion-rate, e.g., SDSS, R11; Shen et al. 2011). Future work (S. Bisogni et al. 2016, in preparation) is aimed at formulating new calibrations for single-epoch C IV-based masses that will account for these large C IV blueshifts and better account for other non-virial components, such as the non-variable, low-velocity core (see Denney 2012), based on a sample of objects with reliable redshift measurements and spanning the diversity of observed quasar properties. However, the ultimate usefulness of such a tool will require that the redshifts of the application sample also be reliably determined so that the C IV-blueshift correction can be accurately applied.

5. CONCLUDING REMARKS

Detailed studies of quasars have clearly shown that there is significant diversity in their spectroscopically observed properties. The most prominent differences, captured by the EV1 parameter space (Boroson & Green 1992), have been linked to physical differences in the quasar environment, most likely determined by the accretion rate. The observed spectroscopic diversity of the relative shifts between the peaks of quasar emission lines is argued to be related to the strength of disk winds that can be driven at high accretion rates (see R11 and references therein). The relation between the observed spectroscopic properties of quasars and the accretion rate leads to correlations of observed quasar spectroscopic properties, in particular relative emission line velocity shifts and ratios, with luminosity in flux-limited samples. As a consequence, determining redshifts for quasars is not as straightforward as determining redshifts for galaxies if the desired precision is $\lesssim$10^3 km s^{-1}. This is because the mean quasar spectrum changes as a function of redshift due to the observed luminosity dependence of the emission-line properties.

In this work, we investigated the degree to which this observed spectroscopic quasar diversity affects redshift determinations for the sample of $z > 1.46$ SDSS-RM quasars by using redshifts based on the He II λ1640 emission-line centroid. We are not advocating that He II ultimately be used as a general tool for determining high redshifts. Its reliability depends on the identification of the narrow component that is only present in some quasars, since the peak wavelength of broad He II is also susceptible to shifts across EV1 parameter space in the absence of a narrow-line component. Furthermore, He II is often low-EW, and therefore cannot always be cleanly isolated in lower-S/N "survey-quality" spectra. Nonetheless, it has benefits for estimating high-z quasar redshifts within the constraints on its observed properties that are set by physically motivated quasar diversity characteristics.

We found that He II-based redshifts in the SDSS-RM sample are consistent, on average, with [O II]-based redshifts within the measurement uncertainties on the line center measurements and the bootstrap estimates of the uncertainty in the sample distribution median. Observed shifts larger than these uncertainties are predominately found in the brightest quasars. [O II]-based redshifts should not be susceptible to line shifts due to the diversity in quasar physical properties deep within the nucleus, which causes the velocity shifts primarily in the broad and/or high-ionization lines, because it is emitted from gas from much larger radii and/or from elsewhere in the quasar host. The $Q = 1$ objects, those with the most reliable He II redshifts, showed a median He II blueshift with respect to [O II] of only 146 km s^{-1}, which is well within the median statistical uncertainty of the PrepSpec [O II] measurements. This suggests that the redshifts of high-redshift quasars with strong narrow He II can be reliably determined to this level of precision from this line alone. The distributions of He II-to-[O II] velocity shifts for the full sample suggest that He II exhibits, on average, a small blueshift with respect to the systemic quasar rest frame, on the order of a couple hundred km s^{-1}, assuming that [O II] is a better proxy for this. However, the He II–[O II] shifts can be large if the emission-line peak of He II cannot be attributed to emission from the NLR. These shifts are not enough to explain the full bias in the BOSS redshifts indicated by this investigation.

By comparing BOSS-pipeline redshifts to our He II-based redshifts, we found evidence that the BOSS-pipeline redshifts are biased, possibly overestimating the redshifts of some high-z quasars by $\sim$1000 km s^{-1}, on average (see Figure 4), while underestimating the redshifts of a smaller population because of the imprint of the physical quasar diversity on observed spectroscopic properties. The main goal of the BOSS survey to measure BAO in the Lyα forest of high-z quasars (e.g., Delubac et al. 2015) did not depend on quasar redshifts having a precision greater than this limit, so the great success of the BOSS survey in that regard is unaffected by these results. However, BOSS spectra are now being used for myriad other purposes that this apparent bias may impact if studies require redshifts to higher precision than this measured systematic difference.

The likely source of this bias in the SDSS-pipeline redshifts is their basis on a comparison to (or in the case of the BOSS pipeline, from a PCA training set that ultimately has redshifts determined from) composite quasar spectra. In the creation of such spectra, objects that exhibit systematic emission-line shifts are coadded with those that do not. This creates an "averaging" effect in terms of the location of the peaks of quasar emission lines. Because the shifts between the lines depend on luminosity for flux-limited samples, the degree of bias introduced depends on how closely the observed spectroscopic properties of the sample used for making the quasar composite resemble the properties of the sample to which it is applied.

We investigated the impact of these redshift biases on physical diagnostics of quasars based on C IV emission-line shifts. Adopting the He II-based redshifts for our sample results in a broader distribution of C IV blueshifts than that found for the HW10-corrected SDSS-pipeline redshifts (see R11). We find a median for our sample that is statistically consistent with zero blueshift within our measurement uncertainties, for objects with a strong He II narrow component, and an extended tail to large blueshifts, dominated by objects with little or no narrow He II line emission. This general picture is consistent with other current studies using more sophisticated redshift determination methods for high-z quasars (P. Hewett 2016, private communication) and with a physical picture where SED-dependent effects can cause a range in C IV blueshifts, but where C IV blueshifts are not ubiquitous across the quasar population within the precision probed by our study.

Our results suggest that future improvements in quasar template-based redshift determinations could potentially be made by creating multiple templates along the Eigenvector 1 (EV1) sequence of quasars properties that spans the observed spectroscopic diversity of quasars. Template selection for each quasar can then be made by comparing as many measurable spectroscopic properties as possible that have been found to relate to EV1 properties, e.g., line ratios, emission-line shapes, line EW, luminosity, continuum slope, X-ray soft excess and power-law slope, etc. (Boroson & Green 1992). Alternatively, for PCA-based redshifts, efforts should be made to formulate a PCA training set composed of quasars covering this same EV1 parameter space, but for which the spectra of each training-set quasar is of high S/N and covers both UV and optical rest wavelengths. Both requirements are important so that the redshifts of the training set are as robust as possible (e.g., based on multiple, unblended narrow emission lines and/or host-galaxy absorption lines, which are often of low EW and require high-quality data to isolate).

We are grateful to Yue Shen for producing the coadded SDSS-RM spectra used in this work and to C. S. Kochanek for discussions and editorial contributions. We thank P. Hewett and G. T. Richards for stimulating discussions that improved the content and clarity of this work. K.D.D. is supported by an NSF AAPF fellowship awarded under NSF grant AST-1302093. K.H. acknowledges support from STFC grant ST/M001296/1. W.N.B. acknowledges support from NSF grant AST-1516784. C.J.G. acknowledges support from NSF grant AST-1517113. B.M.P. is grateful for support from NSF grant AST-1008882. K.H. acknowledges support from STFC grant ST/M001296/1. L.C.H. thanks Carnegie Observatories for providing telescope access and acknowledges financial support from Peking University, the Kavli Foundation, the Chinese Academy of Science through grant No. XDB09030102 (Emergence of Cosmological Structures) from the Strategic Priority Research Program, and from the National Natural Science Foundation of China through grant No. 11473002. J.R.T. acknowledges support from NASA through Hubble Fellowship grant #51330 awarded by the Space Telescope Science

Institute, which is operated by the Association of Universities for Research in Astronomy, Inc., for NASA under contract NAS 5-26555. Funding for SDSS-III has been provided by the Alfred P. Sloan Foundation, the Participating Institutions, the National Science Foundation, and the U.S. Department of Energy Office of Science. The SDSS-III web site is http://www.sdss3.org/. SDSS-III is managed by the Astrophysical Research Consortium for the Participating Institutions of the SDSS-III Collaboration including the University of Arizona, the Brazilian Participation Group, Brookhaven National Laboratory, University of Cambridge, Carnegie Mellon University, University of Florida, the French Participation Group, the German Participation Group, Harvard University, the Instituto de Astrofisica de Canarias, the Michigan State/Notre Dame/JINA Participation Group, Johns Hopkins University, Lawrence Berkeley National Laboratory, Max Planck Institute for Astrophysics, Max Planck Institute for Extraterrestrial Physics, New Mexico State University, New York University, Ohio State University, Pennsylvania State University, University of Portsmouth, Princeton University, the Spanish Participation Group, University of Tokyo, University of Utah, Vanderbilt University, University of Virginia, University of Washington, and Yale University.

REFERENCES

Assef, R. J., Denney, K. D., Kochanek, C. S., et al. 2011, ApJ, 742, 93
Baldwin, J., Ferland, G., Korista, K., & Verner, D. 1995, ApJL, 455, L119
Baskin, A., & Laor, A. 2005, MNRAS, 356, 1029
Baskin, A., Laor, A., & Hamann, F. 2013, MNRAS, 432, 1525
Bolton, A. S., Schlegel, D. J., Aubourg, É., et al. 2012, AJ, 144, 144
Boroson, T. A., & Green, R. F. 1992, ApJS, 80, 109
Bowler, R. A. A., Hewett, P. C., Allen, J. T., & Ferland, G. J. 2014, MNRAS, 445, 359
Busca, N. G., Delubac, T., Rich, J., et al. 2013, A&A, 552, A96
Casebeer, D. A., Leighly, K. M., & Baron, E. 2006, ApJ, 637, 157
Cassinelli, J. P., & Castor, J. I. 1973, ApJ, 179, 189
Dawson, K. S., Kneib, J.-P., Percival, W. J., et al. 2016, AJ, 151, 44
Dawson, K. S., Schlegel, D. J., Ahn, C. P., et al. 2013, AJ, 145, 10
Delubac, T., Bautista, J. E., Busca, N. G., et al. 2015, A&A, 574, A59
Denney, K. D. 2012, ApJ, 759, 44
Denney, K. D., Horne, K., Brandt, W. N., et al. 2016, ApJS, 224, 14
Eisenstein, D. J., Weinberg, D. H., Agol, E., et al. 2011, AJ, 142, 72
Fine, S., Croom, S. M., Bland-Hawthorn, J., et al. 2010, MNRAS, 409, 591
Font-Ribera, A., Arnau, E., Miralda-Escudé, J., et al. 2013, JCAP, 5, 18
Gunn, J. E., Siegmund, W. A., Mannery, E. J., et al. 2006, AJ, 131, 2332
Hewett, P. C., & Wild, V. 2010, MNRAS, 405, 2302
Khare, P., Berk Daniel, V., Rahmani, H., & York, D. G. 2014, ApJ, 794, 66
Korista, K., Baldwin, J., Ferland, G., & Verner, D. 1997, ApJS, 108, 401
Laor, A., Bahcall, J. N., Jannuzi, B. T., et al. 1994, ApJ, 420, 110
Leighly, K. M. 2004, ApJ, 611, 125
Luo, B., Brandt, W. N., Hall, P. B., et al. 2015, ApJ, 805, 122
Marziani, P., Sulentic, J. W., Dultzin-Hacyan, D., Calvani, M., & Moles, M. 1996, ApJS, 104, 37
Marziani, P., Sulentic, J. W., Plauchu-Frayn, I., & del Olmo, A. 2013, ApJ, 764, 150
Murray, N., Chiang, J., Grossman, S. A., & Voit, G. M. 1995, ApJ, 451, 498
Nestor, D., Hamann, F., & Rodriguez Hidalgo, P. 2008, MNRAS, 386, 2055
Netzer, H., Lira, P., Trakhtenbrot, B., Shemmer, O., & Cury, I. 2007, ApJ, 671, 1256
Pâris, I., Petitjean, P., Aubourg, É., et al. 2014, A&A, 563, A54
Park, D., Woo, J.-H., Denney, K. D., & Shin, J. 2013, ApJ, 770, 87
Plotkin, R. M., Shemmer, O., Trakhtenbrot, B., et al. 2015, ApJ, 805, 123
Richards, G. T., Kruczek, N. E., Gallagher, S. C., et al. 2011, AJ, 141, 167
Schneider, D. P., Richards, G. T., Hall, P. B., et al. 2010, AJ, 139, 2360
Shen, Y., Brandt, W. N., Dawson, K. S., et al. 2015, ApJS, 216, 4
Shen, Y., Brandt, W. N., Denney, K. D., et al. 2016, ApJ, 831, 7
Shen, Y., Greene, J. E., Strauss, M. A., Richards, G. T., & Schneider, D. P. 2008, ApJ, 680, 169
Shen, Y., & Liu, X. 2012, ApJ, 753, 125
Shen, Y., Richards, G. T., Strauss, M. A., et al. 2011, ApJS, 194, 45
Smee, S. A., Gunn, J. E., Uomoto, A., et al. 2013, AJ, 146, 32
Sulentic, J. W., Bachev, R., Marziani, P., Negrete, C. A., & Dultzin, D. 2007, ApJ, 666, 757
Sulentic, J. W., Marziani, P., Dultzin-Hacyan, D., Calvani, M., & Moles, M. 1995, ApJL, 445, L85
Vanden Berk, D. E., Richards, G. T., Bauer, A., et al. 2001, AJ, 122, 549
Vestergaard, M., & Peterson, B. M. 2006, ApJ, 641, 689
Wills, B. J., Brotherton, M. S., Fang, D., Steidel, C. C., & Sargent, W. L. W. 1993, ApJ, 415, 563
Woo, J.-H., Bae, H.-J., Son, D., & Karouzos, M. 2016, ApJ, 817, 108
York, D. G., Adelman, J., Anderson, J. E., Jr., et al. 2000, AJ, 120, 1579